

Two-loop radiative seesaw, muon $g - 2$, and τ -lepton-flavor violation with DM constraints

Chuan-Hung Chen^{1,2,*} and Takaaki Nomura^{3,4,†}

¹*Department of Physics, National Cheng-Kung University, Tainan 70101, Taiwan*

²*Physics Division, National Center for Theoretical Sciences, Taipei 10617, Taiwan*

³*School of Physics, KIAS, Seoul 02455, Korea*

⁴*College of Physics, Sichuan University, Chengdu 610065, China*

(Dated: October 4, 2021)

Abstract

The quartic scalar coupling λ_5 term, which violates the lepton-number by two units in the Ma-model, is phenomenologically small when the model is applied to the lepton-flavor violation (LFV) processes. In order to dynamically generate the λ_5 parameter through quantum loop effects and retain the dark matter (DM) candidate, we extend the Ma-model by adding a Z_2 -odd vector-like lepton doublet and a Z_2 -even Majorana singlet. With the new couplings to the Higgs and gauge bosons, the observed DM relic density can be explained when the upper limits from the DM-nucleon scattering cross sections are satisfied. In addition to the neutrino data and LFV constraints, it is found that the DM relic density can significantly exclude the free parameter space. Nevertheless, the resulting muon $g - 2$ mediated by the inert charged-Higgs can fit the 4.2σ deviation between the experimental measurement and the SM result, and the branching ratio for $\tau \rightarrow \mu\gamma$ can be as large as the current upper limit when the rare $\mu \rightarrow (e\gamma, 3e)$ decays are suppressed. In addition, it is found that the resulting $BR(\tau \rightarrow \mu\rho)$ can reach the sensitivity of Belle II with an integrated luminosity of $50 ab^{-1}$.

*e-mail: physchen@mail.ncku.edu.tw

†Electronic address: nomura@scu.edu.cn

I. INTRODUCTION

A radiative seesaw mechanism with a scotogenic scenario for explaining the neutrino mass was proposed in [1], where an inert Higgs doublet (H_I) and three Z_2 -odd Majorana fermions (N_k) were introduced to the standard model (SM). It was found that the essential new effect in [1] is the non-self-Hermitian quartic scalar coupling term, expressed as $\lambda_5(H^\dagger H_I)^2$, in which the lepton number is violated by two units. In addition to providing an explanation for the neutrino data, the model in [1] (called the Ma-model hereafter) can provide the dark matter (DM) candidate, such as the lightest inert neutral scalar or Majorana fermion [1, 2]. Intriguingly, the Ma-model can originate from a larger gauge symmetry, such as $SO(10)$ [3, 4].

When the Ma-model is applied to the detectable lepton-flavor violation (LFV) processes, the λ_5 value has to be an order of $O(10^{-7} - 10^{-9})$ [1, 5]. Although the phenomenologically small parameter can be attributed to the protection of lepton-number symmetry, it can be also taken as a hint that the λ_5 parameter originates from a loop-induced effect [6]; that is, the neutrino mass can be effectively taken as a two-loop effect.

There is a long-standing anomaly in the muon anomalous magnetic dipole moment (muon $g - 2$). The result observed by the E821 experiment at Brookhaven National Lab (BNL) is shown as [7]:

$$a_\mu^{\text{BNL}} = 116592089(63) \times 10^{-11}. \quad (1)$$

The E989 experiment at Fermilab recently reports the first measurement with run-1 data as [8]:

$$a_\mu^{\text{FNAL}} = 116592040(54) \times 10^{-11}. \quad (2)$$

The combined experimental value is $a_\mu^{\text{exp}} = 116592061(41) \times 10^{-11}$ with the uncertainty of 0.35 ppm. Compared to the SM result of $a_\mu^{\text{SM}} = 116591810(43) \times 10^{-11}$ [9], the new result indicates that the deviation between experiment and theory is

$$\Delta a_\mu = a_\mu^{\text{exp}} - a_\mu^{\text{SM}} = (251 \pm 59) \times 10^{-11}, \quad (3)$$

and has reached a significance of 4.2σ .¹ If the anomaly is confirmed, the muon $g - 2$ is a clear signal of a new physics effect [11–46].

¹ The latest lattice QCD calculation for the leading hadronic vacuum polarization from the BMW collaboration, which leads to a larger a_μ , can be found in [10].

A small λ_5 parameter leads to an approximate mass degeneracy between the neutral scalars in H_I . Thus, the muon $g - 2$, which arises from the inert scalar and pseudoscalar bosons in Ma-model, is canceled; in addition, the inert charged-Higgs contribution is negative and cannot explain the observation shown in Eq. (3). Hence, in order to resolve the muon $g - 2$ anomaly together with neutrino physics, a slight extension of the Ma-model is necessary.

In this study, we investigate a minimal extension of the Ma-model in such a way that the muon $g - 2$ anomaly can arise from the inert charged-Higgs mediation, where the λ_5 term is absent at the tree level and is induced via a one-loop effect. It is found that the goal can be achieved when a Z_2 -odd vector-like lepton doublet X and a Z_2 -even Majorana fermion (N_0) are added to the Ma-model.

When λ_5 vanishes at the tree level, the scalar potential in the Ma-model has a global $U(1)$ symmetry, denoted as $U(1)_\chi$. With proper $U(1)_\chi$ charge assignments, although the $U(1)$ symmetry is softly broken by the Majorana fermion mass terms in the Yukawa sector, a residual Z_2 symmetry is retained in the full Lagrangian. Thus, similar to the Ma-model, (H_I, N_k, X) are Z_2 -odd, whereas N_0 is a Z_2 -even. Thus, using the $N_k N_k (N_0 N_0)$ Majorana terms and the new Yukawa couplings $X_L H_I N_0$ and $X_L H N_k$, the Z_2 -even $\lambda_5 (H^\dagger H_I)^2$ term can be induced via box diagrams.

Since the masses between the inert scalar bosons are approximately degenerate, and the Z gauge coupling to the neutral component X^0 of X is somewhat large, these Z_2 -odd particles are not suitable as the DM candidates due to the strict DM direct detection constraints. Thus, the most favorable DM candidate in the model is the lightest N_k . One of the main tasks in this work is to examine whether the obtained DM relic density in the model can fit the current Planck result [47] when the experimental upper limits of the DM direct detection [48–50] are satisfied.

In addition to the neutrino, the muon $g - 2$, and the DM relic density issues, it is of interest to determine whether the model can lead to sizable LFV processes, such as $\tau \rightarrow \mu\gamma$, $\tau \rightarrow 3\mu$, and $\tau \rightarrow \ell(P, V)$, where P and V denote the possible pseudoscalar and vector mesons, respectively. As shown in [5], the LFV processes arising from the photon-penguin diagrams are much larger than those from the Z -penguin diagrams. We find that the branching ratio (BR) for $\tau \rightarrow \mu\gamma$ in the model can be as large as the current upper limit of 4.4×10^{-8} [61], whereas the result of $\tau \rightarrow 3\mu$ can reach a magnitude of the order of 10^{-10} . Although the $\mu \rightarrow e\gamma$ and $\mu \rightarrow 3e$ processes and the $\mu - e$ conversion can create a

strict constraint on the free parameters, since the constrained parameters can be ascribed to the electron-related parameters, we thus assume that the related parameter value vanishes in order to simplify the numerical analysis. We will show that the vanished parameter can be taken as a cancellation among the parameters. Therefore, in this study, the $\mu \rightarrow e\gamma$, $\mu \rightarrow 3e$, and $\tau \rightarrow e\gamma$ decays are suppressed. A detailed analysis can be found in [5].

From our analysis, it is found that when we only take the neutrino data as the constraints, the allowed parameter space, which can lead to a large $BR(\tau \rightarrow \mu\gamma)$, is wide; however, when the obtained parameter space is applied to the DM relic density, although $BR(\tau \rightarrow \mu\gamma)$ of $O(10^{-8})$ can be still achieved, the allowed parameter space is significantly reduced; that is, the observed DM relic density can further restrict the parameter space. Using the constrained parameter values, it is found that $BR(\tau \rightarrow \mu\rho^0)$ can reach $O(10^{-10})$.

Since our study concentrates on the flavor physics, the neutrino physics, and the issue as to whether a Z_2 -odd particle can be a weakly interactive massive particle (WIMP), and the observed DM relic density can be explained in the scotogenic model, we thus skip the detailed analysis for the signal search at the LHC; instead, we briefly discuss the production cross sections and the associated collider signals of the Z_2 -odd charged leptons. The relevant collider signals for the inert scalars and fermions can be found in [62–69].

The paper is organized as follows: In addition to the extension of the Ma-model, in Sec. II, we discuss the new Yukawa couplings, the flavor mixings between X^0 and N_k , the neutrino mass matrix element constraints, and the gauge couplings to the Z_2 -odd particles in detail. In Sec. III, we study the constraints from the DM direct detections and search for the allowable parameter space that can fit the observed DM relic density. The study of the LFV processes and the muon $g - 2$ is shown in Sec. IV. A summary is given in Sec. V.

II. MODEL AND RELEVANT COUPLINGS

In this section, we discuss the extension of the Ma-model and derive the relevant couplings of DM to the SM particles.

A. The Model

In order to dynamically generate the λ_5 parameter in Ma-model, we introduce a global $U(1)_\chi$ symmetry to suppress the tree-level λ_5 term in the scalar potential, where the SM particles do not carry the $U(1)_\chi$ charge. Since the $\lambda_5(H^\dagger H_I)^2$ term breaks the lepton-number by two units, it is natural to extend the model by introducing new particles to the lepton sector. Since the inert Higgs H_I in the model is an $SU(2)_L$ doublet, due to the $SU(2)_L \times U(1)_Y \times U(1)_\chi$ invariance in the Lagrangian, the minimal extension, which is a chiral anomaly-free, is to add one vector-like lepton doublet (X) to the Ma-model.

Although new couplings are introduced, such as $\bar{X}_L H_I \ell_R$, the lepton-number symmetry is still retained. The lepton-number violation can be achieved if a right-handed Majorana fermion (N_0) is added to the Ma-model, where N_0 carries the lepton-number. Thus, the lepton-number can be broken by the Majorana mass term. The charge assignments for the new particles under $SU(2)_L \times U(1)_Y \times U(1)_\chi$ are given in Table I, where $N_{1,2,3}$ are the singlet fermions in the original Ma-model. In section II C, we discuss in detail how the lepton violating effect generates the λ_5 parameter. In the next subsection, we will demonstrate that $U(1)_\chi$ is softly broken to a Z_2 symmetry by the dimension-3 Majorana mass term. Hence, H_I , $N_{1,2,3}$, and X are Z_2 -odd, and N_0 is a Z_2 -even.

TABLE I: Representations and charge assignments of the introduced particles.

Particle	$SU(2)_L \times U(1)_Y$	$U(1)_\chi$	Z_2
X	(2, -1)	1	-
$N_{1,2,3}$	(1, 0)	1	-
N_0	(1, 0)	2	+
H_I	(2, 1)	1	-

B. Yukawa couplings and flavor mixings

Since the loop-induced λ_5 term relies on the Yukawa interactions, we first discuss the Yukawa couplings involved and the resulting flavor mixings between X^0 and N_k ($k=1,2,3$), in which the mixing effects are strongly correlated to the muon $g-2$ and the DM detections.

The gauge invariant lepton Yukawa couplings under $SU(2)_L \times U(1)_Y \times U(1)_\chi$ symmetry can be written as:

$$\begin{aligned}
-\mathcal{L}_Y = & \bar{L}\mathbf{y}^\ell H\ell_R + \bar{L}\mathbf{y}_L^{\prime k}\tilde{H}_I N_k + \bar{X}_L\mathbf{y}'_R H_I\ell_R + \bar{X}_L h_L^k \tilde{H} N_k + y_L^0 \bar{X}_L \tilde{H}_I N_0 \\
& + m_X \bar{X}_L X_R + \frac{m_{N_k}}{2} \bar{N}_k^C N_k + \frac{m_{N_0}}{2} \bar{N}_0^C N_0 + H.c., \tag{4}
\end{aligned}$$

where the lepton flavor indices are suppressed; H is the SM Higgs doublet, and $N^C = C\gamma^0 N^*$ with $C = i\gamma^0\gamma^2$, $\tilde{H}_{(I)} = i\tau_2 H_{(I)}^*$, and m_{N_k} , m_X , and m_{N_0} are the masses of N_k , X , and N_0 , respectively. Since $\bar{L}HN_0$ is a dimension-4 interaction and is a hard $U(1)_\chi$ symmetry breaking term, the induced λ_5 parameter has an ultraviolet (UV) divergence; thus, the hard breaking effect has to be excluded at the tree level. We only allow the soft $U(1)_\chi$ breaking term existing in the Lagrangian such that the loop-induced effect is UV finite. Accordingly, the neutrino masses are all generated through loop effects. It can be easily found that using the transformations $N_0 \rightarrow e^{i2\theta_\chi} N_0$ and $N_k \rightarrow e^{i\theta_\chi} N_k$, the Majorana mass terms $N_k^T N_k$ and $N_0^T N_0$ break the global $U(1)_\chi$ symmetry; however, the symmetry is not completely broken. It can be seen that a Z_2 symmetry is retained when $\theta_\chi = \pi$. As a result, X , N_k , and H_I under the residual symmetry are transformed as:

$$(X, N_k, H_I) \longrightarrow e^{i\pi}(X, N_k, H_I). \tag{5}$$

That is, X , N_k , and H_I are Z_2 -odd particles, where H_I is the so-called inert-Higgs doublet [2].

Using the taken expressions:

$$H = \begin{pmatrix} G^+ \\ (\phi^0 + iG^0)/\sqrt{2} \end{pmatrix}, \quad H_I = \begin{pmatrix} H_I^+ \\ (S_I + iA_I)/\sqrt{2} \end{pmatrix}, \quad X = \begin{pmatrix} X^0 \\ X^- \end{pmatrix}, \tag{6}$$

the Yukawa interactions from Eq. (4) can be written as:

$$\begin{aligned}
-\mathcal{L}_Y \supset & h_L^k \bar{X}_L^0 N_k \frac{v+h}{\sqrt{2}} + \left(\bar{X}_L^0 \mathbf{y}_R \ell_R - \bar{N}_k \mathbf{y}_L^{k\dagger} \ell_L - y_L^{0*} \bar{N}_0 X_L^- \right) H_I^+ \\
& + \left(\bar{X}_L^- \mathbf{y}_R \ell_R + \bar{N}_k \mathbf{y}_L^{k\dagger} \nu_L + y_L^{0*} \bar{N}_0 X_L^0 \right) \frac{S_I + iA_I}{\sqrt{2}} \\
& + m_X \left(\bar{X}_L^0 X_R^0 + \bar{X}_L^- X_R^- \right) + \frac{m_{N_k}}{2} \bar{N}_k^C N_k + \frac{m_{N_0}}{2} \bar{N}_0^C N_0 + H.c., \tag{7}
\end{aligned}$$

where we have dropped the unphysical Goldstone bosons and the SM interactions. $\phi^0 = (v+h)/\sqrt{2}$ is used for the SM Higgs, where v is the vacuum expectation value (VEV) of ϕ^0 . Since X^- is a Z_2 -odd particle, it cannot mix with the SM charged leptons after electroweak

symmetry breaking (EWSB). Thus, the SM charged-lepton masses are still dictated by the first term in Eq. (4), where we can introduce the unitary matrixes $U_{R,L}^\ell$ to diagonalize the mass matrix by $m_{\ell_i} = (U_L^\ell \mathbf{y}^\ell U_L^{\ell\dagger})_{ii} v / \sqrt{2}$. With the introduced $U_{R,L}^\ell$, the couplings in $\bar{L} \mathbf{y}'^k \tilde{H}_I N_k$ and $\bar{X}_L \mathbf{y}'_R H_I \ell_R$ can be written as:

$$\mathbf{y}_L^k = U_L^\ell \mathbf{y}_L'^k, \quad \mathbf{y}_R = \mathbf{y}'_R U_R^{\ell\dagger}. \quad (8)$$

Due to the flavor mixing effects, the \mathbf{y}_{Ri} (\mathbf{y}_{Li}^k) couplings can in general have very different magnitudes in different flavors when the differences in \mathbf{y}'_{Rj} (\mathbf{y}_{Lj}^k) are only in one to two orders of magnitude; that is, Eq. (8) shows that the parameter cancellations are technically allowed. This is quite different from the λ_5 issue, where the involved parameter is only λ_5 itself.

From Eq. (7), it can be seen that X^0 and N_k can mix through the SM Higgs after EWSB. Due to the mixings, the chirality-flipped electromagnetic dipole operators, which contribute to the radiative LFV and the lepton $g - 2$, can be radiatively induced by the mediation of the charged inert-Higgs H_I^\pm without the suppression of m_ℓ . Since the $X_{R(L)}$ mass term is a Dirac type, in order to form a multiplet state with N_k , we rewrite the Dirac mass form to be the Majorana mass form as:

$$m_X \bar{X}_L X_R = \frac{1}{2} (\bar{X}_R^C, \bar{X}_L) \begin{pmatrix} 0 & m_X \\ m_X & 0 \end{pmatrix} \begin{pmatrix} X_R \\ X_L^C \end{pmatrix}. \quad (9)$$

Thus, the mass matrix for $(X_R, X_L^C, N_1, N_2, N_3)$ can be written as:

$$M_{XN} = \begin{pmatrix} 0 & m_X & \mathbf{0}_{1 \times 3} \\ m_X & 0 & \mathbf{m}_{\mathbf{XN}} \\ \mathbf{0}_{3 \times 1} & \mathbf{m}_{\mathbf{XN}}^T & (\mathbf{m}_N)_{3 \times 3} \end{pmatrix}, \quad (10)$$

with $(\mathbf{m}_{\mathbf{XN}})^k = v h_L^k / \sqrt{2}$ and $(\mathbf{m}_N)_{3 \times 3} = \text{diag}(m_{N_1}, m_{N_2}, m_{N_3})$. The 5×5 M_{XN} matrix can be diagonalized by introducing a unitary matrix (V), i.e., $M_{XN}^{\text{dia}} = V M_{XN} V^T$. To simplify the formulation of the physical masses in terms of m_X , m_{N_k} , and h_L^k , we take $m_0 = m_{N_k}$. Based on the approximation proposed in [28], the five eigenvalues of the Majorana states can be parametrized as:

$$\begin{aligned} m_1 &\approx -m_X - (\delta m_X - \delta m_N), \quad m_2 \approx m_X + \delta m_X, \\ m_{3(4)} &= m_0, \quad m_5 \approx m_0 - \delta m_N, \end{aligned} \quad (11)$$

with

$$\begin{aligned}\delta m_X &= \frac{M_\eta^2}{m_X - m_0/\sqrt{2}}, \\ M_\eta^2 &= \frac{v^2}{2} \sum_k (h_L^k)^2, \\ \delta m_N &= m_X + \delta m_X - \sqrt{m_X^2 + M_\eta^2},\end{aligned}\quad (12)$$

where the mass identities obey the trace and determinant invariances, i.e. $\text{Tr}(M_{XN}) = \sum_i m_i$, and $\det(M_{XN}) = \prod_i m_i$, and the mass eigenstates are denoted as χ_{iR} and χ_{iR}^C ($i = 1 \sim 5$). Since X^0 is not suitable as a DM candidate due to a large coupling to Z -boson, we take the mass order to be $m_0 < m_X$ and set m_5 as the lightest Z_2 -odd fermion mass in the model. Using the obtained eigenvalues, the flavor mixing matrix can be approximately formulated as:

$$V \approx \begin{pmatrix} \frac{m_X}{\mathcal{N}_1|m_1|} & -\frac{1}{\mathcal{N}_1} & \frac{m_{XN}^1}{2m_0\mathcal{N}_1} & \frac{m_{XN}^2}{2m_0\mathcal{N}_1} & \frac{m_{XN}^3}{2m_0\mathcal{N}_1} \\ \frac{m_X}{\mathcal{N}_2m_2} & \frac{1}{\mathcal{N}_2} & -\frac{m_{XN}^1}{\mathcal{N}_2(m_0-m_2)} & -\frac{m_{XN}^2}{\mathcal{N}_2(m_0-m_2)} & -\frac{m_{XN}^3}{\mathcal{N}_2(m_0-m_2)} \\ 0 & 0 & \frac{m_{XN}^2}{\mathcal{N}_3\sqrt{(m_{XN}^1)^2+(m_{XN}^2)^2}} & -\frac{m_{XN}^1}{\mathcal{N}_3\sqrt{(m_{XN}^1)^2+(m_{XN}^2)^2}} & 0 \\ 0 & 0 & \frac{m_{XN}^1}{\mathcal{N}_4\sqrt{(m_{XN}^1)^2+(m_{XN}^2)^2}} & \frac{m_{XN}^2}{\mathcal{N}_4\sqrt{(m_{XN}^1)^2+(m_{XN}^2)^2}} & -\frac{\sqrt{(m_{XN}^1)^2+(m_{XN}^2)^2}}{\mathcal{N}_4m_{XN}^3} \\ \frac{m_X}{\mathcal{N}_5m_5} & \frac{1}{\mathcal{N}_5} & -\frac{m_{XN}^1}{\mathcal{N}_5(m_0-m_5)} & -\frac{m_{XN}^2}{\mathcal{N}_5(m_0-m_5)} & \frac{m_{XN}^3}{\mathcal{N}_5(m_0-m_5)} \end{pmatrix}, \quad (13)$$

where \mathcal{N}_a ($a = 1 \sim 5$) are the normalization factors and satisfy $\sum_i V_{ai}^2 = 1$.

By the linear combination of χ_{iR} and χ_{iR}^C , we can define the Majorana states as $\chi_i = \chi_{iR} + \chi_{iR}^C$, where $\chi_i^C = \chi_i$. In terms of χ_i , the h Yukawa couplings to χ_i can be derived as:

$$\begin{aligned}-\mathcal{L}_{h\chi} &= \bar{\chi}_i Y_{ij}^h \chi_j h, \\ Y_{ij}^h &= \sum_{k=1}^3 \frac{h_L^k}{2\sqrt{2}} (V_{i2} V_{k+2}^\dagger + V_{ik+2} V_{2j}^\dagger),\end{aligned}\quad (14)$$

whereas the inert scalar couplings are expressed as:

$$\begin{aligned}-\mathcal{L}_Y \supset & \left(\overline{X_L^-} \mathbf{y}_R \ell_R + \overline{\chi}_j V_{jk+2} \mathbf{y}_L^{k\dagger} \nu_L + y_L^{0*} V_{2j}^\dagger \overline{N}_0 \chi_j \right) \frac{S_I + iA_I}{\sqrt{2}} \\ & + \left(\overline{\chi}_j V_{j2} \mathbf{y}_R \ell_R - \overline{\chi}_j V_{jk+2} \mathbf{y}_L^{k\dagger} \ell_L - y_L^{0*} \overline{N}_0 X_L^- \right) H_I^+ + H.c.\end{aligned}\quad (15)$$

From Eq. (14), when χ_5 is the lightest Z_2 -odd fermion, it can cause spin-independent (SI) DM-nucleon scattering. Furthermore, in addition to the h -mediated χ_5 annihilation process, the couplings in Eqs. (14) and (15) can contribute to the relic density of DM via the coannihilation processes.

C. Loop induced λ_5 and scalar masses

The scalar potential, which follows the $SU(2)_L \times U(1)_Y \times U(1)_X$ symmetry, can be written as [1, 2]:

$$V(H, H_I) = \mu^2 H^\dagger H + \lambda_1 (H^\dagger H)^2 + m_I^2 H_I^\dagger H_I + \lambda_2 (H_I^\dagger H_I)^2 + \lambda_3 (H^\dagger H)(H_I^\dagger H_I) + \lambda_4 (H^\dagger H_I)(H_I^\dagger H). \quad (16)$$

It can be seen that the essential non-self-Hermitian λ_5 term, which is defined by:

$$V_5 = \frac{\lambda_5}{2} [(H^\dagger H_I)^2 + H.c.] , \quad (17)$$

is suppressed. To generate the λ_5 term through one-loop effects, the $U(1)_X$ breaking effects have to be involved. From the Yukawa sector, it is known that the dimension-3 Majorana mass terms m_{N_k} and m_{N_0} can be as the $U(1)_X$ breaking source. The one-loop Feynman diagram used to generate the $(H^\dagger H_I)^2$ term is sketched in Fig. 1. Using the Yukawa couplings shown in Eq. (7), the loop-induced λ_5 parameter can be obtained as:

$$\lambda_5 = -8 \sum_k \left(\frac{h_L^k y_L^{0*}}{4\pi} \right)^2 \frac{m_{N_0} m_{N_k}}{m_X^2} J(x_k, x_0), \quad (18)$$

$$J(a, b) = \frac{1}{2(1-a)(1-b)} + \frac{1}{2(a-b)} \left[\frac{a^2 \ln a}{(1-a)^2} - \frac{b^2 \ln b}{(1-b)^2} \right],$$

with $x_k = m_{N_k}^2/m_X^2$ and $x_0 = m_{N_0}^2/m_X^2$. In addition to the dependence of the h_L^k and y_L^0 Yukawa couplings, the resulting λ_5 is associated with the $m_{N_k} m_{N_0}$ factor. For a numerical illustration, if we take $m_X = 1$ TeV, $m_{N_k} = 800$ GeV, $m_{N_0} = 100$ GeV, $h_L^k = 0.5$, and $y_L^0 = 0.02$, the induced- λ_5 value can be estimated as $\lambda_5 \approx -3.45 \times 10^{-7}$.

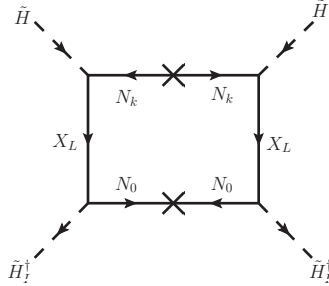


FIG. 1: Feynman diagram used to produce the $\lambda_5(H^\dagger H_I)^2$ term, where $\tilde{H}_I^\dagger \tilde{H} = H^\dagger H_I$.

When the λ_5 term in Eq. (17) is added to Eq. (16), the scalar potential is the same as that in the inert-Higgs model [1, 2]. Thus, the (S, A, H^\pm) masses are obtained as:

$$m_{S_I}^2 = m_I^2 + \lambda_L v^2, \quad m_{A_I}^2 - m_{S_I}^2 = -\lambda_5 v^2, \quad m_{H_I^\pm}^2 = m_I^2 + \frac{\lambda_3}{2} v^2, \quad (19)$$

with $\lambda_L = (\lambda_3 + \lambda_4 + \lambda_5)/2 \approx (\lambda_3 + \lambda_4)/2$. Since the resulting λ_5 is negative in the model, we have $m_{A_I} > m_{S_I}$ although the mass difference is very small.

D. Allowed regions for the Majorana neutrino mass matrix elements

With the exception of the loop-induced λ_5 , the neutrino mass generation mechanism in the study is the same as that in the Ma-model, where the effective two-loop Feynman diagram is shown in Fig. 2. Thus, according to the results in [1], the Majorana neutrino mass matrix elements can be written as [1, 70]:

$$m_{ij}^\nu = \sum_k \frac{y_{L_i}^k y_{L_j}^k}{2(4\pi)^2} m_{N_k} \left[\frac{m_{A_I}^2 \ln(m_{A_I}^2/m_{N_k}^2)}{m_{N_k}^2 - m_{A_I}^2} - \frac{m_{S_I}^2 \ln(m_{S_I}^2/m_{N_k}^2)}{m_{N_k}^2 - m_{S_I}^2} \right], \quad (20)$$

where the λ_5 -parameter is hidden in the mass difference between m_{A_I} and m_{S_I} , as shown in Eq. (19). It can be found that m_{ij}^ν can be of $O(10^{-2})$ eV when $\sum_k y_{L_i}^k y_{L_j}^k \sim O(10^{-4} - 10^{-3})$ and $m_{S_I(A_I)} \approx m_{N_k} \approx 1$ TeV are used. Eq. (20) can be diagonalized using the Pontecorvo-Maki-Nakagawa-Sakata (PMNS) matrix as:

$$m_{ij}^\nu = U_{\text{PMNS}}^* m_\nu^{\text{diag}} U_{\text{PMNS}}^\dagger, \quad (21)$$

where $m_\nu^{\text{diag}} = \text{diag}(m_1, m_2, m_3)$, and U_{PMNS} can be parametrized as:

$$U_{\text{PMNS}} = \begin{pmatrix} c_{12}c_{13} & s_{12}c_{13} & s_{13}e^{-i\delta} \\ -s_{12}c_{23} - c_{12}s_{23}s_{13}e^{i\delta} & c_{12}c_{23} - s_{12}s_{23}s_{13}e^{i\delta} & s_{23}c_{13} \\ s_{12}s_{23} - c_{12}c_{23}s_{13}e^{i\delta} & -c_{12}s_{23} - s_{12}c_{23}s_{13}e^{i\delta} & c_{23}c_{13} \end{pmatrix} \\ \times \text{diag}(1, e^{i\alpha_{21}/2}, e^{i\alpha_{31}/2}), \quad (22)$$

in which $s_{ij} \equiv \sin \theta_{ij}$ and $c_{ij} \equiv \cos \theta_{ij}$; δ is the Dirac CP violating phase, and $\alpha_{21,31}$ are Majorana CP violating phases.

Although the neutrino mass ordering is not yet conclusive, due to the insensitivity to the mass ordering, we use the normal ordering (NO) scenario to illustrate the numerical results.

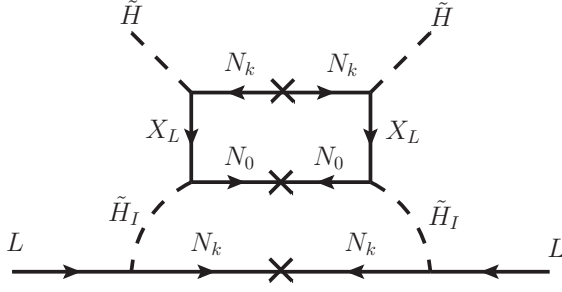


FIG. 2: Two-loop diagram for the Majorana neutrino mass.

Based on the neutrino oscillation data, the central values of θ_{ij} , δ , and Δm_{ij}^2 , which are obtained from a global fitting approach, can be shown as [71]:

$$\begin{aligned} \theta_{12} &= 34.5^\circ, \theta_{23} = 47.7^\circ, \theta_{13} = 8.45^\circ, \delta = 218^\circ, \\ \Delta m_{21}^2 &= 7.55 \times 10^{-5} \text{ eV}^2, \Delta m_{31}^2 = 2.50 \times 10^{-3} \text{ eV}^2, \end{aligned} \quad (23)$$

where $m_1 = 0$ for NO is applied, and the Majorana phases are taken to be $\alpha_{21(31)} = 0$. Taking 3σ uncertainties, the magnitudes of the Majorana matrix elements in units of eV can be obtained as:

$$(m_{ij}^\nu)_{\text{NO}} \approx \begin{pmatrix} 0.11 - 0.45 & 0.12 - 0.82 & 0.12 - 0.82 \\ 0.12 - 0.82 & 2.4 - 3.3 & 2.0 - 2.2 \\ 0.12 - 0.82 & 2.0 - 2.2 & 2.2 - 3.1 \end{pmatrix} \times 10^{-2}. \quad (24)$$

When we scan all parameter spaces, the values in Eq. (24) are taken as inputs to bound the free parameters.

E. Z_2 -odd fermion gauge couplings

The Z_2 -odd X is an $SU(2)_L$ doublet, where the strength of the electroweak gauge coupling to X^0 is similar to that to the SM leptons; therefore, X^0 is not suitable for a DM candidate. However, the lightest $SU(2)_L$ singlet N_k can couple to the Z -gauge boson through the flavor mixings V_{ij} which are suppressed by $h^k v / (\sqrt{2} m_X)$. Thus, the lightest Z_2 -odd neutral fermion (χ_5) has the potential to be the DM candidate, where the DM relic density can be explained when the constraint from the DM-nucleon scattering experiments are satisfied. To study

the DM-related phenomena, we formulate the X couplings to W^\pm , Z , and A_μ as:

$$\begin{aligned} \mathcal{L}_{XV} = & -\frac{g}{\sqrt{2}} [\bar{\chi}_i \gamma^\mu (V_{i1} P_R + V_{i2} P_L) X^- W_\mu^+ + H.c.] \\ & + \bar{X}^- \gamma_\mu X^- V_1^\mu - \frac{g c_{ij}^Z}{2 \cos \theta_W} \bar{\chi}_i \gamma^\mu \frac{\gamma_5}{2} \chi_j Z_\mu, \end{aligned} \quad (25)$$

where the Majorana states χ_i are applied; $c_{ij}^Z = V_{i1} V_{j1} - V_{i2} V_{j2}$, and V_1^μ is defined as:

$$V_1^\mu = e A^\mu - \frac{g}{2 \cos \theta_W} (2 \sin^2 \theta_W - 1) Z^\mu.$$

It can be seen that χ_5 can couple to the Z -gauge boson through an axial-vector current, in which the interaction leads to spin-dependent (SD) DM-nucleon scattering. Also, in addition to the Z -mediated χ_5 annihilation processes, the other couplings in Eq. (25) can contribute to the DM relic density via the coannihilation processes.

III. ANALYSIS OF THE DM RELIC DENSITY AND THE DM DIRECT DETECTIONS

A. Constraint from the DM relic density

In the model, the DM candidates can be χ_5 and S_I . However, when $\lambda_5 \sim 10^{-7}$ and $m_{A_I} - m_{S_I} \sim \text{keV}$, a large DM-nucleon scattering cross-section via the $S_I A_I Z$ gauge coupling can be induced [2]. Thus, we consider the χ_5 Majorana fermion as the DM candidate and take the inert Higgs scalar masses to be the scale of $O(\text{TeV})$. In the numerical estimation of the DM relic density, the S_I , A_I , and H_I^\pm contributions are all taken into account. In order to determine if χ_5 can be dark matter, we now examine whether the associated couplings can produce the observed DM relic density (Ω_{DM}), in which the observed value is given as [47]:

$$\Omega_{\text{DM}}^{\text{obs}} h^2 = 0.11933 \pm 0.00091. \quad (26)$$

Since Ω_{DM} is inversely proportional to the thermal average of the product of the DM annihilation cross section and its velocity, i.e., $\langle \sigma v \rangle$, in addition to the DM annihilation and co-annihilation cross sections, we have to consider the thermal effects, which are dictated by the Boltzmann equations. In order to deal with these effects, we implement the model to micrOMEGAs [72] and select the unitary gauge when we use the code for estimating the numerical results. The main parameters for producing Ω_{DM} in the DM annihilation and

coannihilation processes are h_L^k and m_{X,N_k} . Since \mathbf{y}_L^k and y_L^0 are related to the radiative corrections to the neutrino masses and the λ_5 parameter, respectively, their contributions are small and can be ignored. The inert scalar contributions to Ω_{DM} are dictated by \mathbf{y}_R and $m_{S_I(A_I),H_I^\pm}$; however, it is found that when $m_{S_I(A_I),H_I^\pm} \gtrsim 900$ GeV, their effects are small. Hence, to estimate Ω_{DM} , we fix $m_X = m_{H_I^\pm} = m_{S_I(A_I)} = 1000$ GeV and vary the h_L^k and m_0 parameters in the following regions:

$$h_L^k = [-0.5, 0.5], \quad m_0 = [500, 1000] \text{ GeV}, \quad (27)$$

where the step sizes for Δh_L^k and Δm_0 in the calculations are set at 0.1 and 20 GeV, respectively.

We plot the resulting $\Omega_{\text{DM}} h^2$ as a function of m_{χ_5} in Fig. 3(a), where the solid lines are the $\Omega_{\text{DM}}^{\text{obs}} h^2$ result with 5σ errors. From the results, we can find the allowed parameter values to fit the observed DM relic density. In addition, it can be seen that $\Omega_{\text{DM}}^{\text{obs}} h^2$ can give a strict limit on the h_L^k parameters. For the purpose of clarity, we show the $\Omega_{\text{DM}} h^2 - m_{\chi_5}$ plot with $h_L^2 = 0.2$ and $h_L^3 = 0.3$ in Fig. 3(b), where the dotted, dashed, and dash-dotted lines are $h_L^1 = 0.2, 0.3,$ and 0.35 , respectively. We note that the dominant channels for $\Omega_{\text{DM}} h^2$ depend on the h_L^k couplings and the DM mass. For instance, in Fig. 3(b), the main contribution for $\Omega_{\text{DM}} h^2 \geq \Omega_{\text{DM}}^{\text{obs}} h^2$ is from the annihilation channel $\chi_5 \chi_5 \rightarrow Zh$; however, the situation for $\Omega_{\text{DM}} h^2 < \Omega_{\text{DM}}^{\text{obs}} h^2$ in a heavier DM region is dominated by the coannihilation channels, where the involved processes are related to X^\pm and χ_i and the associated cross-sections are somewhat large.

B. SI and SD DM-nucleon scatterings

We have shown that $\Omega_{\text{DM}}^{\text{obs}} h^2$ can be explained in the model when χ_5 is the DM candidate. Since no DM signals are found in the SI [48] and SD [49, 50] DM-nucleon scatterings, the DM direct detections may provide a strict constraint on the free parameters. To examine whether the allowed parameter space, which can fit $\Omega_{\text{DM}}^{\text{obs}} h^2$, is excluded by the current experimental upper limits, in the following, we discuss the contributions to the DM-nucleon scattering cross-sections.

From the interactions in Eqs. (14) and (25), the four-Fermi effective interactions for the

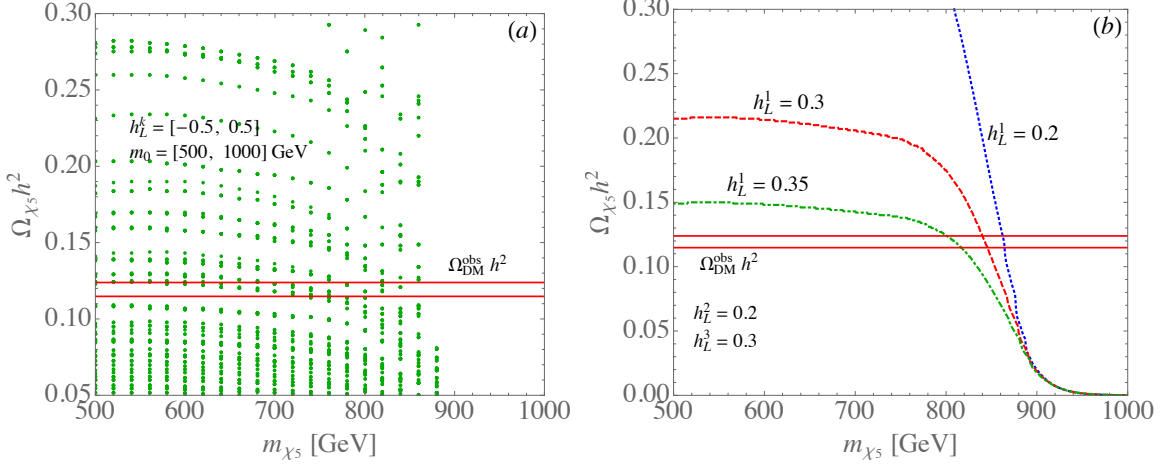


FIG. 3: $\Omega_{\text{DM}} h^2$ as a function of m_{χ_5} , where (a) $h_L^k = [-0.5, 0.5]$ is used; (b) $h_L^2 = 0.2$ and $h_L^3 = 0.3$ are fixed, and $h_L^1 = (0.2, 0.3, 0.35)$ are shown by the dotted, dashed, and dash-dotted lines, respectively. In both plots, $m_0 = [500, 1000]$ GeV is used, and the observed $\Omega_{\text{DM}} h^2$ with 5σ errors is shown.

χ_5 -DM scattering off the SM quarks via the h - and Z -mediation can be expressed as:

$$\begin{aligned}
\mathcal{H}_{\chi_5 N} \supset & -\frac{Y_{55}^h}{v m_h^2} \bar{\chi}_5 \chi_5 \sum_q m_q \bar{q} q \\
& + \sqrt{2} G_F c_{55}^Z \bar{\chi}_5 \gamma^\mu \gamma_5 \chi_5 \sum_q \bar{q} \gamma_\mu (g_V^q + g_A^q \gamma_5) q, \\
g_V^u = & \frac{g}{2 \cos \theta_W} \left(\frac{1}{2} - \frac{4}{3} s_W^2 \right), \quad g_A^u = -\frac{1}{2}, \\
g_V^d = & \frac{g}{2 \cos \theta_W} \left(-\frac{1}{2} + \frac{2}{3} s_W^2 \right), \quad g_A^d = \frac{1}{2},
\end{aligned} \tag{28}$$

where g_V^f and g_A^f denote the Z couplings to the SM quarks. Accordingly, the h -mediated SI DM-nucleon scattering cross-section can be expressed as [73]:

$$\sigma_h^{SI} \approx \frac{|Y_{55}^h|^2}{4\pi} \frac{m_N^2 \mu_{\chi_5 N}^2 f_N^2}{v^2 m_h^4}, \tag{29}$$

where $f_N \approx 0.3$, and $\mu_{\chi_5 N} = m_{\chi_5} m_N / (m_{\chi_5} + m_N)$ is the DM-nucleon reduced mass. The Z -mediated SD DM-nucleon scattering cross-section can be obtained as [74]:

$$\sigma_Z^{SD} \approx \frac{6 G_F^2 \mu_{\chi_5 N}^2}{\pi} |c_{55}^Z|^2 [g_A^u \Delta_u^N + g_A^d (\Delta_d^N + \Delta_s^N)]^2, \tag{30}$$

where the quark spin fractions of the nucleon are taken as $\Delta_u^N = -0.43$, $\Delta_d^N = 0.85$, and $\Delta_s^N = -0.08$ [72].

Before numerically showing the constraint from the observed SI (SD) DM-nucleon cross-section, we first study the event rates of the DM-nucleus scattering, which arise from the DM-spin independent and dependent nonrelativistic operators. In order to obtain the coefficients of the nonrelativistic Galilean invariant effective operators, we use the package *DirectDM* [51–56], where the renormalization group (RG) effects are included. We employ the package *DMFormFactor* [57, 58] to estimate the nucleus transition matrix element in the DM-nucleus scattering amplitude. The event number with an exposure time (T) can be obtained as:

$$N = \int \frac{dR_D}{dE_R} \frac{T}{2m_T} dE_R, \quad (31)$$

where dR_D/dE_R is the event rate, m_T is the nucleus mass, and E_R is the nucleus recoil energy. Taking ^{131}Xe , 278.8×1.3 t kilogram days, and the allowed parameter values constrained by $\Omega_{DM}^{\text{obs}} h^2$, the resulting event number ratio of SD to SI as a function of m_{χ_5} is shown in Fig. 4. From the result, it can be seen that the SI cross-section is larger than the SD cross-section by a factor of 10^4 . The result of $N_{SD} \ll N_{SI}$ can be simply understood as follows. For the contributions from the DM-spin independent effective operators, the DM can be taken to coherently couple to the entire nucleus; thus, the scattering amplitude can be enhanced by the nucleus mass number, i.e., $A_{X_e} = 131$ in our case.

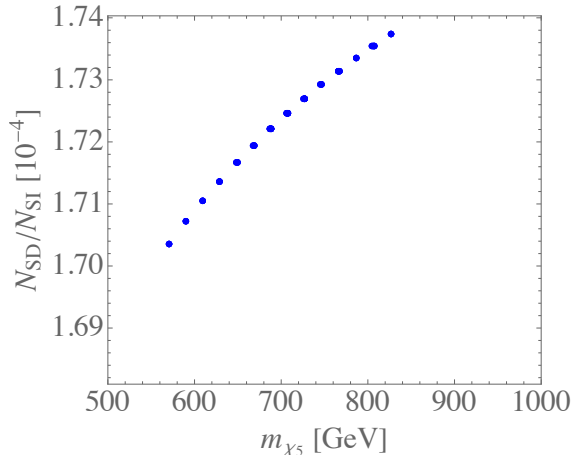


FIG. 4: Event number ratio of SD contribution to SI contribution in DM- ^{131}Xe scattering.

Since SI effects predominantly contribute to the DM-nucleus cross-section, in the following, we only take the SI data measured by XENON1T [48] as the constraint. To estimate the SI DM-nucleon cross-section in the model, in addition to applying Eq. (29), we can also

use the differential cross-section through the relation, defined by [60]:

$$\frac{d\sigma}{dq^2} = \frac{\sigma_{\chi_5 N}^{\text{SI}} A_{\text{Xe}}^2}{4\mu_{\chi_5 N}^2 v_i^2} F(q^2), \quad (32)$$

where $F(q^2)$ can be the Helm form factor with $F(0) = 1$ [59], and v_i is the incident DM velocity. Then, the SI DM-nucleon cross-section $\sigma_{\chi_5 N}^{\text{SI}}$ can be obtained at zero momentum transfer. We show the SI DM-nucleon cross-section as a function of m_{χ_5} in Fig. 5, where the constraint from $\Omega_{\text{DM}}^{\text{obs}} h^2$ is applied, and the dash-dotted line is the upper bound taken from the XENON1T experiment shown in [48]. The filled circles are calculated from Eq. (29), and the squares are the results from the DM-nucleus scattering calculated by using *DMFormfactor*. It can be seen that although the calculations from Eq. (29) are somewhat larger than those from *DMFormfactor*, both results are well below the experimental upper limit.

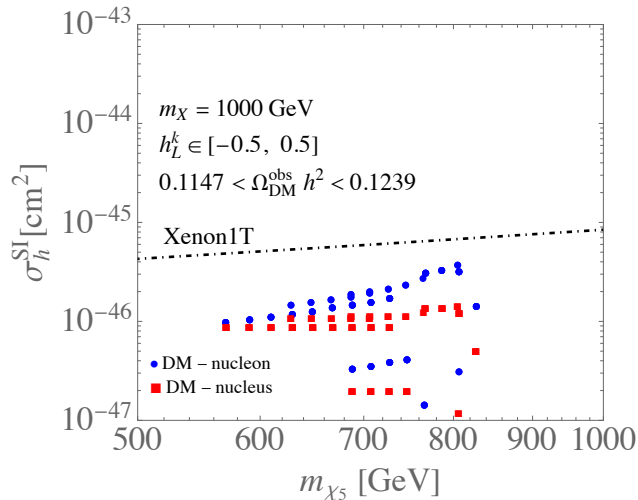


FIG. 5: Scatters for σ_h^{SI} as a function of m_{χ_5} , where the constraint from $\Omega_{\text{DM}}^{\text{obs}} h^2$ is applied, and the current upper bounds for the SI DM-nucleon scatterings is taken from the XENON1T experiments in [48]. The dotted points are obtained from Eq. (29), and the squares are obtained though DM-nucleus scattering calculated by using *DMFormfactor*

IV. LFV, MUON $g - 2$, AND NUMERICAL ANALYSIS

According to earlier discussions, it is known that the \mathbf{y}_L^k parameters can be constrained by the neutrino data when the m_{S_i} and m_0 values are properly taken, whereas the h_L^k and

m_0 parameters can be bounded by the DM relic density when m_X is fixed. In addition, the loop-induced λ_5 is related to h_L^k , $m_{0,X}$, m_{N_0} , and y_L^0 , where we can freely choose the m_{N_0} and y_L^0 values to obtain the expected λ_5 value. In the following study, we investigate the influence of these parameters on the LFV processes and the muon $g - 2$.

A. Formulations of the $\ell_i \rightarrow \ell_j \gamma$, the muon $g - 2$, and the $\tau \rightarrow \ell V$ decays.

The LFV processes in the model arise from the loop effects, such as the γ - and Z -penguin, and box diagrams. Although the LFV processes can be induced by the $S_I(A_I)$ -mediated penguin diagrams, because of $\lambda_5 \ll 1$ and $m_{S_I} \approx m_{A_I}$, the S_I and A_I contributions cancel each other and are small. Due to $\mathbf{y}_L^k \sim 10^{-3} - 10^{-2}$, the box diagrams contributing to the $\ell_i \rightarrow 3\ell_j$ decays are small and negligible in the model [28]. We note that our situation is different from that shown in [5], where the importance of the box diagrams is based on $\mathbf{y}_L^k \sim O(1)$. Therefore, the main contributions to LFV in the model are from the H_I^\pm -mediated penguin diagrams.

Although the Z -penguin diagrams can contribute to $\ell_i \rightarrow 3\ell_j$, their effects are smaller than those in the photon-penguin [28]; thus, we only show the photon-penguin contributions and ignore the Z -penguin effects in the numerical analysis. The photon-penguin Feynman diagrams are sketched in Fig. 6. Since the left panel is only associated with the right-handed lepton couplings y_{Ri} , due to the chirality-flip, the resulting decay amplitude has an m_{ℓ_i} suppression factor. The right panel involves left- and right-handed couplings, i.e., $y_{Li}^k y_{Rj}$ and $y_{Ri} y_{Lj}^k$, at the same time, therefore, these are the dominant effects used to generate the LFV processes.

Following Fig. 6 and the introduced Yukawa couplings, the effective interactions for $\ell_i \rightarrow \ell_j \gamma$ can be written as:

$$\mathcal{L}_{\ell_i \rightarrow \ell_j \gamma} = \frac{e}{2} m_{\ell_i} \bar{\ell}_j \sigma_{\mu\nu} (C_L^{ji} P_L + C_R^{ji} P_R) \ell_i F^{\mu\nu}, \quad (33)$$

where $m_{\ell_j} = 0$ is taken, and the Wilson coefficients and loop integral functions are obtained

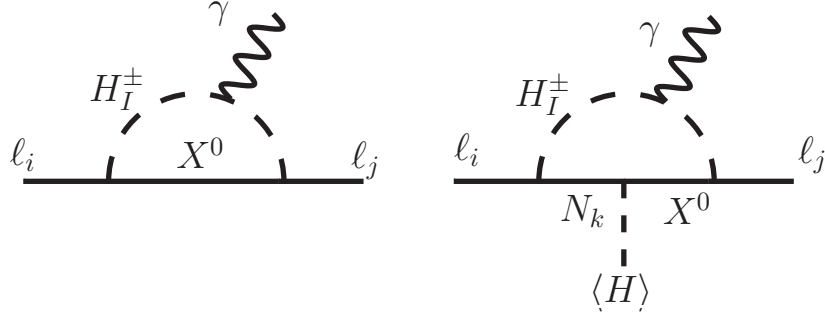


FIG. 6: Feynman diagrams for the $l_i \rightarrow l_j \gamma$ decays, where the decay amplitude in the left panel has an m_{ℓ_i} suppression factor due to chirality-flip. The right panel exhibits the left- and right-handed couplings at the same time, and no chiral suppression is involved.

as:

$$C_L^{ji} = \frac{y_{Rj} y_{Ri}}{16\pi^2} \sum_{t=1}^5 \frac{V_{t2}^2}{m_{\chi_t}^2} I_1^\gamma \left(\frac{m_{H_I^\pm}^2}{m_{\chi_t}^2} \right) + \frac{y_{Rj}}{16\pi^2 m_{\ell_i}} \sum_{t=1}^5 \sum_{k=1}^3 \frac{V_{t2} V_{tk+2} y_{Lj}^k}{m_{\chi_t}} I_2^\gamma \left(\frac{m_{H_I^\pm}^2}{m_{\chi_t}^2} \right), \quad (34)$$

$$C_R^{ji} = \frac{y_{Ri}}{16\pi^2 m_{\ell_i}} \sum_{t=1}^5 \sum_{k=1}^3 \frac{V_{t2} V_{tk+2} y_{Lj}^k}{m_{\chi_t}} I_2^\gamma \left(\frac{m_{H_I^\pm}^2}{m_{\chi_t}^2} \right), \quad (35)$$

$$I_1^\gamma(a) = \frac{a^2 - 5a - 2}{12(1-a)^3} + \frac{a \ln a}{2(1-a)^4},$$

$$I_2^\gamma(a) = \frac{1+a}{2(1-a)^2} + \frac{a \ln a}{(1-a)^3}.$$

As a result, the BR for $l_i \rightarrow l_j \gamma$ can be expressed as:

$$BR(l_i \rightarrow l_j \gamma) = \tau_{\ell_i} \frac{\alpha m_{\ell_i}^5}{4} (|C_L^{ji}|^2 + |C_R^{ji}|^2), \quad (36)$$

with $\alpha = e^2/4\pi$.

It is known that the lepton $g-2$ originates from the radiative quantum corrections, where the associated form factors are written as:

$$\Gamma^\mu = \bar{\ell}(p') \left[\gamma^\mu F_1(k^2) + \frac{i\sigma^{\mu\nu} k_\nu}{2m_\ell} F_2(k^2) \right] \ell(p), \quad (37)$$

and the lepton $g-2$ is defined as:

$$a_\ell = \frac{g_\ell - 2}{2} = F_2(0). \quad (38)$$

As discussed earlier, the left panel in Fig. 6 has an extra m_μ suppression factor relative to the right panel. If the left panel contribution is dropped, the dominant lepton $g - 2$ in the model can be obtained as:

$$a_\ell = -\frac{m_\ell y_{R\ell}}{16\pi^2} \sum_{t=1}^5 \sum_{k=1}^3 \frac{V_{t2} V_{tk+2} y_{L\ell}^k}{m_{\chi_t}^2} I_2^\gamma \left(\frac{m_{H_I^\pm}^2}{m_{\chi_t}^2} \right). \quad (39)$$

The photon-penguin, which induces the $\tau \rightarrow \ell\gamma^*$ decays, can also contribute to the hadronic two-body decays, such as $\tau \rightarrow \ell\rho^0$ and $\tau \rightarrow \ell\phi$. Because of the vector-current conservation, the $\tau \rightarrow \ell\pi^0$ decays are suppressed. Similarly, since the flavor state of ω -meson is $(u\bar{u} + d\bar{d})/\sqrt{2}$, $\tau \rightarrow \ell\omega$ is suppressed due to the electric charge cancellation between the u - and d -quarks. Hence, we only focus on the $\tau \rightarrow \ell(\rho^0, \phi)$ decays.

From the Yukawa couplings to the inert charged-Higgs shown in Eq. (15), the effective interaction for $\tau \rightarrow \ell\gamma^*$ can be obtained as:

$$\mathcal{L}_{\tau\ell\gamma^*} = m_\tau \frac{y_{R3} y_{R\ell}}{16\pi^2} \sum_{t=1}^5 \frac{V_{t2}^2}{m_{\chi_t}^2} I_3^\gamma \left(\frac{m_{H_I^\pm}^2}{m_{\chi_t}^2} \right) p_\tau \cdot \epsilon_\gamma^* \bar{\ell} P_L \tau, \quad (40)$$

where ϵ_γ^μ denotes the photon polarization vector, and the loop integral is given as:

$$I_3^\gamma(a) = -\frac{3a-1}{(a-1)^2} + \frac{2a^2 \ln a}{(a-1)^3}. \quad (41)$$

Using the vector meson decay constant, defined by:

$$\langle 0 | \bar{q} \gamma^\mu q' | V \rangle = m_V f_V \epsilon_V^\mu, \quad (42)$$

the decay amplitude for $\tau \rightarrow \ell V$ is written as:

$$M(\tau \rightarrow \ell V) = m_\tau \frac{y_{R3} y_{R\ell} \alpha_{\text{em}}}{4\pi} \sum_{t=1}^5 \frac{V_{t2}^2}{m_{\chi_t}^2} I_3^\gamma \left(\frac{m_{H_I^\pm}^2}{m_{\chi_t}^2} \right) \frac{f_V^2}{m_V^2} \epsilon_V^* \cdot p_\tau \bar{\ell} P_L \tau, \quad (43)$$

with $\alpha_{\text{em}} = e^2/4\pi$. Thus, the BR for the $\tau \rightarrow \ell V$ decay can be formulated as:

$$\begin{aligned} BR(\tau \rightarrow \ell V) &= \frac{m_\tau}{128\pi} \left[\frac{\alpha_{\text{em}} y_{R3} y_{R2}}{4\pi} \sum_{t=1}^5 V_{t2}^2 I_3^\gamma \left(\frac{m_{H_I^\pm}^2}{m_{\chi_t}^2} \right) \frac{m_\tau^2}{m_{\chi_t}^2} \right]^2 \\ &\times \frac{m_\tau^2}{m_V^2} \frac{f_V^2}{m_V^2} \left(1 - \frac{m_V^2}{m_\tau^2} \right)^2. \end{aligned} \quad (44)$$

We note that the decay constant of ρ^0 meson can be related to that of ρ^+ , i.e. $f_{\rho^0} = f_{\rho^+}/\sqrt{2}$.

B. Numerical analysis and discussion

In addition to the constraints from the DM relic density and the neutrino data, the rare LFV decays can also strictly constrain the involved parameters, for which the selected experimental upper limits are given in Table II. From Eqs. (34) and (35), it can be seen that the $\ell_i \rightarrow \ell_j \gamma$ decays are related to the y_{Li}^k , h_L^k , and y_{Ri} parameters, where the y_{Li}^k and h_L^k are used to fit the $\Omega_{\text{DM}}^{\text{obs}} h^2$ and $(m_{ij}^\nu)_{\text{NO}}$ results. Thus, to satisfy the upper limits of the rare $\mu \rightarrow e\gamma, 3e$ decays, we simply take $y_{R1} = 0$ and $\sum_k h_L^k y_{L1}^k = 0$. Then, $\mu \rightarrow (e\gamma, 3e)$ and $\tau \rightarrow (e\gamma, 3e)$ are suppressed, and y_{L1}^1 is determined as:

$$y_{L1}^1 = -\frac{1}{h_L^1} (h_L^2 y_{L1}^2 + h_L^3 y_{L1}^3) . \quad (45)$$

We note that from Eq. (8), a small y_{R1} can be achieved by taking proper U_R^ℓ in such a way that $y_{R1} = y'_{Rj} (U_R^{\ell\dagger})_{j1} \simeq 0$, where the y'_{Rj} values in different flavors can be only different by one to two orders of magnitude.

TABLE II: Current experimental upper limits of the selected LFV processes.

LFV	$\mu \rightarrow e\gamma$	$\mu \rightarrow 3e$	$\tau \rightarrow \mu(e)\gamma$	$\tau \rightarrow 3\mu(3e)$
BR	4.2×10^{-13}	1.0×10^{-12}	$4.4(3.3) \times 10^{-8}$	$2.1(2.7) \times 10^{-8}$

Since the number of free parameters is more than that of the constraints, we cannot independently determine each of them; therefore, we scan all parameters in the chosen regions. For the parameter scans, we fix $m_X = m_{H_I^\pm} = m_{S_I} = 1000$ GeV and $m_0 = 800$ GeV, and the scanned regions are taken as:

$$\begin{aligned} y_{Li}^k &= [-0.06, 0.06] \quad (i \neq 1), \\ h_L^k &= [-0.5, 0.5], \\ y_{R2} &= [-3, 3], \quad y_{R3} = [-1, 1]. \end{aligned} \quad (46)$$

Using 5×10^9 random sampling points, we show the scatter plot for the correlation between the resulting muon $g - 2$ (in units of 10^{-10}) and the y_{R2} parameter in Fig. 7(a), where the bounds, such as $(m_{ij}^\nu)_{\text{NO}}$ shown in Eq. (24), $BR(\tau \rightarrow \mu\gamma) < 4.4 \times 10^{-8}$, and $a_\mu = (5, 30) \times 10^{-10}$, are taken into account. It can be seen that a_μ is sensitive to the y_{R2} parameter. From the result, it can be concluded that with $y_{R2} \sim O(1)$, $a_\mu \sim 20 \times 10^{-10}$

can be achieved. Now, the Fermilab muon $g - 2$ experiment confirms the BNL result. If the muon $g - 2$ anomaly is further confirmed in the future, the inert charged-Higgs mediated effect in the model can be the potential mechanism. The BR for $\tau \rightarrow \mu\gamma$ (in units of 10^{-8}) as a function of y_{R3} is shown in Fig. 7(b), where the resulting $BR(\tau \rightarrow \mu\gamma)$ can be as large as the current upper limit. It can be found that when $y_{R3} = 0$, $BR(\tau \rightarrow \mu\gamma)$ is not suppressed because the dominant contribution is from the right panel in Fig. 6, in which the associated effect is $h_L^k y_{L3}^k y_{R2}$. For the purpose of clarity, we also show the correlation of a_μ and $BR(\tau \rightarrow \mu\gamma)$ in Fig. 7(c).

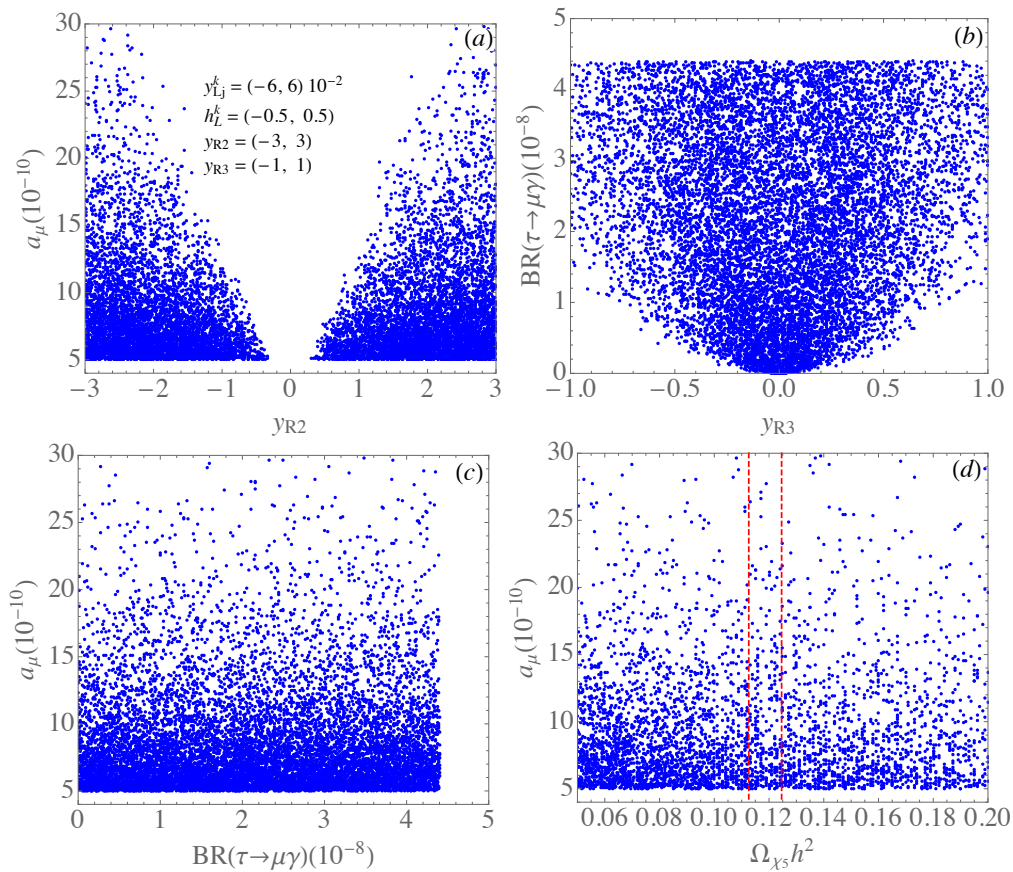


FIG. 7: Scatter plots for the correlation between (a) a_μ and y_{R2} , (b) $BR(\tau \rightarrow \mu\gamma)$ and y_{R3} , (c) a_μ and $BR(\tau \rightarrow \mu\gamma)$, and (d) a_μ and $\Omega_{\text{DM}} h^2$.

The scanning results shown in Fig. 7(a)-(c) have not yet included the $\Omega_{\text{DM}}^{\text{obs}} h^2$ constraint. In order to determine the influence of the DM relic density, we use micrOMEGAs and apply the h_L^k values, which are obtained from Fig. 7(a)-(c), to estimate $\Omega_{\text{DM}} h^2$. As a result, the scatter plot for the correlation between a_μ and $\Omega_{\text{DM}} h^2$ is shown in Fig. 7(d), where the vertical

dashed lines denote the $\Omega_{\text{DM}}^{\text{obs}} h^2$ result with 5σ errors. From the figure, it can be seen that $\Omega_{\text{DM}}^{\text{obs}} h^2$ significantly excludes the parameter space, where the predicted muon $g-2$ can be as large as $a_\mu \sim 20 \times 10^{-10}$. After including the $\Omega_{\text{DM}}^{\text{obs}} h^2$ constraint, the new a_μ - $BR(\tau \rightarrow \mu\gamma)$ result is given in the left panel of Fig. 8. In addition, the result for $BR(\tau \rightarrow 3\mu)$ (in units of 10^{-10}) is shown in the right panel of Fig. 8, where the dominant effect is from the off-shell photon decay, i.e., $\tau \rightarrow \mu\gamma^* \rightarrow 3\mu$. It can be seen that $BR(\tau \rightarrow 3\mu)$ is two orders of magnitude smaller than $BR(\tau \rightarrow \mu\gamma)$ in the model.

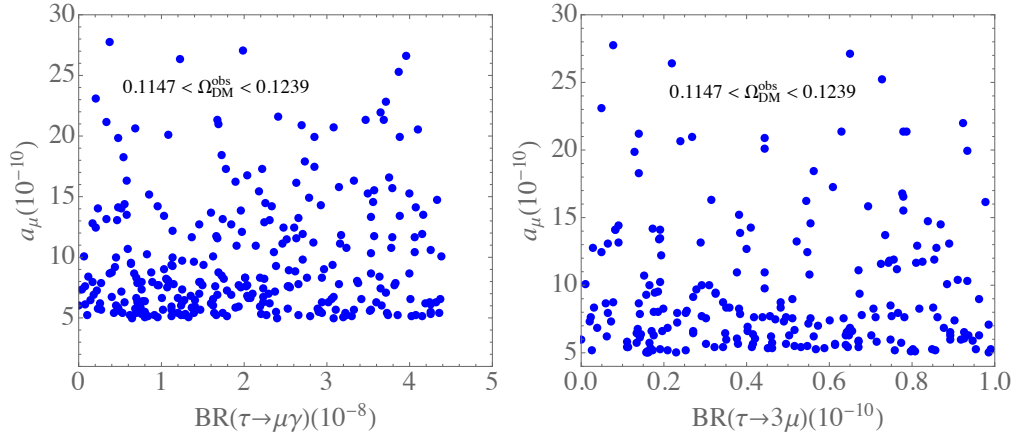


FIG. 8: Scatter plots for the correlation between a_μ and $BR(\tau \rightarrow \mu\gamma)$ [left panel] and $BR(\tau \rightarrow 3\mu)$ [right panel], where the observed $\Omega_{\text{DM}} h^2$ constraint is included.

Since the couplings related to the electron are suppressed in this work, we only numerically discuss the $\tau \rightarrow \mu V$ decays. Using $f_\phi = 0.231$ GeV, $f_{\rho^+} = 0.205$ GeV [75], and Eq. (44), we show the resulting $BR(\tau \rightarrow \mu\phi)$ (left panel) and $BR(\tau \rightarrow \mu\rho^0)$ (right panel) versus a_μ in units of 10^{-10} in Fig. 9, where the allowed parameter values constrained by the observed DM relic density have been taken into account. From the results, it can be seen that both BRs of the rare LFV tau decays can reach the order of 10^{-10} . Due to phase space effect, we have $BR(\tau \rightarrow \mu\phi) < BR(\tau \rightarrow \mu\rho^0)$. The sensitivities in Belle II with the integrated luminosity of $50 ab^{-1}$ can achieve 10^{-9} for the $\mu\phi$ mode and 2×10^{-10} for the $\mu\rho^0$ mode [76]. That is, in addition to the $\tau \rightarrow \mu\gamma$ decay, we can use $\tau \rightarrow \mu\rho^0$ to test the model.

In addition to the flavor physics, we briefly discuss some implications in collider physics. Since the new Z_2 -odd fermions are lighter than the inert-Higgs doublet, we consider the production of Z_2 -odd fermions at the LHC, where the fermions can be produced via the gauge interactions shown in Eq. (25). We focus on the processes producing charged fermions

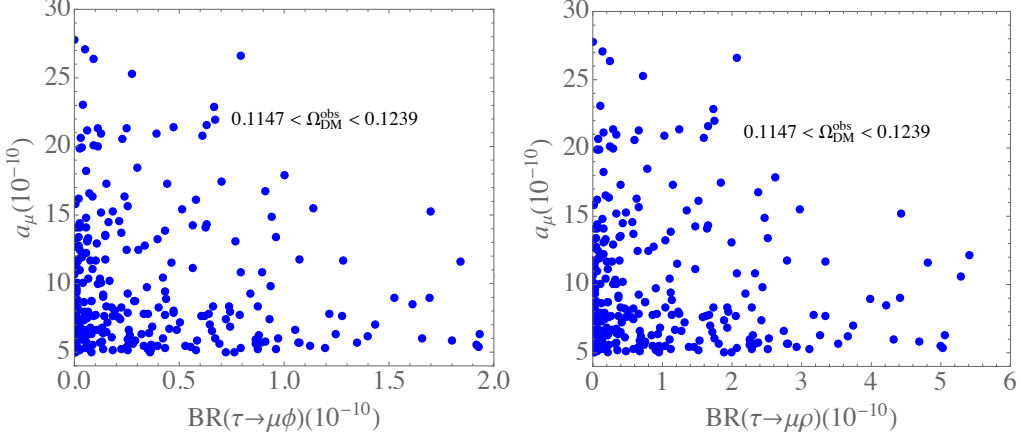


FIG. 9: Scatter plots for a_μ versus $BR(\tau \rightarrow \mu\phi)$ [left panel] and $BR(\tau \rightarrow \mu\rho^0)$ [right panel], where the observed $\Omega_{\text{DM}}h^2$ constraint is taken into account.

and DM, such as:

$$pp \rightarrow W^\pm \rightarrow \chi_5 X^\pm, \quad (47)$$

$$pp \rightarrow Z/\gamma \rightarrow X^+ X^-, \quad (48)$$

where the former processes involve the neutral fermion mixing effects as shown in Eq. (13). To illustrate the collider signature, we take some benchmark points (BPs), which are consistent with the relic density and the considered constraints, as:

$$\begin{aligned} \text{BP1} : h_L^1 &= 0.20, V_{51} = 0.16, V_{52} = 0.13, m_{\chi_5} = 791 \text{ GeV}, \\ \text{BP2} : h_L^1 &= 0.30, V_{51} = 0.18, V_{52} = 0.14, m_{\chi_5} = 788 \text{ GeV}, \\ \text{BP3} : h_L^1 &= 0.35, V_{51} = 0.19, V_{52} = 0.15, m_{\chi_5} = 786 \text{ GeV}, \end{aligned} \quad (49)$$

where $m_X = 1 \text{ TeV}$, $m_0 = 800 \text{ GeV}$, $h_L^2 = 0.20$, and $h_L^3 = 0.30$ are fixed for all BPs.

For the numerical calculations, we employ *CalcHEP* [77]. The resulting cross sections for the taken BPs in the pp collisions at $\sqrt{s} = 14 \text{ TeV}$ are shown as:

$$\begin{aligned} \text{BP1} : \sigma(\chi_5 X^+) &= 0.042 \text{ fb}, \sigma(\chi_5 X^-) = 0.013 \text{ fb}, \sigma(X^+ X^-) = 0.69 \text{ fb}, \\ \text{BP2} : \sigma(\chi_5 X^+) &= 0.052 \text{ fb}, \sigma(\chi_5 X^-) = 0.016 \text{ fb}, \sigma(X^+ X^-) = 0.71 \text{ fb}, \\ \text{BP3} : \sigma(\chi_5 X^+) &= 0.060 \text{ fb}, \sigma(\chi_5 X^-) = 0.019 \text{ fb}, \sigma(X^+ X^-) = 0.71 \text{ fb}. \end{aligned} \quad (50)$$

The difference between $\sigma(\chi_5 X^+)$ and $\sigma(\chi_5 X^-)$ arises from the different production rate between W^+ and W^- . The produced X^\pm predominantly decay into χ_5 and the SM particles

via the off-shell W^\pm , i.e. $X^\pm \rightarrow \chi_5 \bar{f} f'$, where $f(f')$ is the SM fermion. Thus, the clear signals will be $\ell^\pm \cancel{E}_T$ and $\ell^+ \ell^- \cancel{E}_T$, where the former is from $\chi_5 X^\pm$; the latter is from $X^+ X^-$; $\ell = e, \mu$, and \cancel{E}_T is the missing transverse energy. Accordingly, with an integrated luminosity of 3000 fb^{-1} , the signal number of events can be estimated as: $N(\ell^+ \cancel{E}_T) \sim 40$, $N(\ell^- \cancel{E}_T) \sim 10$ and $N(\ell^+ \ell^- \cancel{E}_T) \sim 80$ for BP3. Using the event selection condition with $\cancel{E}_T > 500 \text{ GeV}$, it can be found that the corresponding number of background events can be estimated as $N_{bgs} \sim 600$ for $\ell^+ \ell^- \cancel{E}_T$ [78]; that is, the statistical significance can reach 3σ . Nevertheless, it is worth mentioning that the high-energy LHC with $\sqrt{s} = 27 \text{ TeV}$ can be used to discover the heavy vector-like lepton of $m_X \lesssim 1700 \text{ GeV}$ [79].

V. SUMMARY

A radiative seesaw mechanism, which adds a Z_2 -odd Higgs doublet and three singlet Majorana fermions to the SM, was proposed in [1]. When the neutrino data are satisfied, it is found that the λ_5 quartic scalar coupling in the scalar potential has to be small when the lepton-flavor violation processes are required to fit the upper limits, and the resulting muon anomalous magnetic dipole moment cannot explain the inconsistency between the experimental results and the SM prediction.

In order to explain the small λ_5 parameter based on a dynamic mechanism and enhance the muon $g - 2$, we extended the Ma-model by adding a vector-like lepton doublet X and a Majorana singlet N_0 , where the former is a Z_2 -odd state and the latter is a Z_2 -even particle. The DM candidate in the model is the lightest N_k . Because of the mixings between X and N_k , the DM can scatter off the nucleon through both the spin-independent and -dependent processes. Although no signal is found in the direct detections due to the severe constraints, the modified Ma-model can still fit the observed DM relic density.

It is found that the new couplings $X H N_k$ and $X H_I \ell_R$ in the model not only can enhance muon $g - 2$ to reach a level of 20×10^{-10} , but also can make the branching ratio for $\tau \rightarrow \mu \gamma$ as large as the current upper limit and make it possible for $\tau \rightarrow \mu(\phi, \rho^0)$ to be of the order of 10^{-10} . In this study, we also showed that when the parameter values, which are constrained by the neutrino data and lepton-flavor violation processes, are used to estimate the $\Omega_{\text{DM}} h^2$, the resulting parameter space is significantly shrunk by the observed DM relic density. Although the heavy leptons may not be discovered in the high-luminosity LHC, the

heavy lepton of $m_X \sim 1$ TeV can potentially be found in the high-energy LHC.

Acknowledgments

This work was supported by the Ministry of Science and Technology of Taiwan, under grants MOST-108-2112-M-006-003-MY2.

-
- [1] E. Ma, Phys. Rev. D **73**, 077301 (2006) [hep-ph/0601225].
 - [2] R. Barbieri, L. J. Hall and V. S. Rychkov, Phys. Rev. D **74**, 015007 (2006) [hep-ph/0603188].
 - [3] E. Ma, Phys. Rev. D **98**, no. 9, 091701 (2018) [arXiv:1809.03974 [hep-ph]].
 - [4] E. Ma, arXiv:1810.06506 [hep-ph].
 - [5] T. Toma and A. Vicente, JHEP **1401**, 160 (2014) [arXiv:1312.2840 [hep-ph]].
 - [6] R. Franceschini and R. N. Mohapatra, Phys. Rev. D **89**, no.5, 055013 (2014) [arXiv:1306.6108 [hep-ph]].
 - [7] G. W. Bennett *et al.* [Muon g-2], Phys. Rev. D **73**, 072003 (2006) [arXiv:hep-ex/0602035 [hep-ex]].
 - [8] B. Abi *et al.* [Muon g-2], Phys. Rev. Lett. **126**, 141801 (2021) [arXiv:2104.03281 [hep-ex]].
 - [9] T. Aoyama, N. Asmussen, M. Benayoun, J. Bijnens, T. Blum, M. Bruno, I. Caprini, C. M. Carloni Calame, M. Cè and G. Colangelo, *et al.* Phys. Rept. **887**, 1-166 (2020) [arXiv:2006.04822 [hep-ph]].
 - [10] S. Borsanyi *et al.*, Nature (2021), 2002.12347. [arXiv:2002.12347 [hep-lat]].
 - [11] A. Czarnecki and W. J. Marciano, Phys. Rev. D **64**, 013014 (2001) [hep-ph/0102122].
 - [12] S. N. Gninenko and N. V. Krasnikov, Phys. Lett. B **513**, 119 (2001) [hep-ph/0102222].
 - [13] E. Ma and M. Raidal, Phys. Rev. Lett. **87**, 011802 (2001) Erratum: [Phys. Rev. Lett. **87**, 159901 (2001)] [hep-ph/0102255].
 - [14] C. H. Chen and C. Q. Geng, Phys. Lett. B **511**, 77 (2001) [hep-ph/0104151].
 - [15] E. Ma, D. P. Roy and S. Roy, Phys. Lett. B **525**, 101 (2002) [hep-ph/0110146].
 - [16] R. Benbrik, C. H. Chen and T. Nomura, Phys. Rev. D **93**, no. 9, 095004 (2016) [arXiv:1511.08544 [hep-ph]].
 - [17] T. Nomura and H. Okada, Phys. Lett. B **756**, 295 (2016) [arXiv:1601.07339 [hep-ph]].

- [18] S. Baek, T. Nomura and H. Okada, Phys. Lett. B **759**, 91 (2016) [arXiv:1604.03738 [hep-ph]].
- [19] W. Altmannshofer, M. Carena and A. Crivellin, Phys. Rev. D **94**, no. 9, 095026 (2016) [arXiv:1604.08221 [hep-ph]].
- [20] C. H. Chen, T. Nomura and H. Okada, Phys. Rev. D **94**, no. 11, 115005 (2016) [arXiv:1607.04857 [hep-ph]].
- [21] S. Lee, T. Nomura and H. Okada, Nucl. Phys. B **931**, 179 (2018) [arXiv:1702.03733 [hep-ph]].
- [22] C. H. Chen, T. Nomura and H. Okada, Phys. Lett. B **774**, 456 (2017) [arXiv:1703.03251 [hep-ph]].
- [23] A. Das, T. Nomura, H. Okada and S. Roy, Phys. Rev. D **96**, no. 7, 075001 (2017) [arXiv:1704.02078 [hep-ph]].
- [24] K. Kowalska and E. M. Sessolo, JHEP **1709**, 112 (2017) [arXiv:1707.00753 [hep-ph]].
- [25] L. Calibbi, R. Ziegler and J. Zupan, JHEP **1807**, 046 (2018) [arXiv:1804.00009 [hep-ph]].
- [26] B. Barman, D. Borah, L. Mukherjee and S. Nandi, Phys. Rev. D **100**, no. 11, 115010 (2019) [arXiv:1808.06639 [hep-ph]].
- [27] T. Nomura and H. Okada, arXiv:1903.05958 [hep-ph].
- [28] C. H. Chen and T. Nomura, Phys. Rev. D **100**, no. 1, 015024 (2019) [arXiv:1903.03380 [hep-ph]].
- [29] C. H. Chen and T. Nomura, [arXiv:2001.07515 [hep-ph]].
- [30] C. H. Chen and T. Nomura, Nucl. Phys. B **964**, 115314 (2021) [arXiv:2003.07638 [hep-ph]].
- [31] G. Arcadi, L. Calibbi, M. Fedele and F. Mescia, [arXiv:2104.03228 [hep-ph]].
- [32] X. F. Han, T. Li, H. X. Wang, L. Wang and Y. Zhang, [arXiv:2104.03227 [hep-ph]].
- [33] T. Nomura and H. Okada, [arXiv:2104.03248 [hep-ph]].
- [34] C. H. Chen, C. W. Chiang and T. Nomura, [arXiv:2104.03275 [hep-ph]].
- [35] S. F. Ge, X. D. Ma and P. Pasquini, [arXiv:2104.03276 [hep-ph]].
- [36] Y. Bai and J. Berger, [arXiv:2104.03301 [hep-ph]].
- [37] P. M. Ferreira, B. L. Gonçalves, F. R. Joaquim and M. Sher, [arXiv:2104.03367 [hep-ph]].
- [38] M. Abdughani, Y. Z. Fan, L. Feng, Y. L. Sming Tsai, L. Wu and Q. Yuan, [arXiv:2104.03274 [hep-ph]].
- [39] M. Van Beekveld, W. Beenakker, M. Schutten and J. De Wit, [arXiv:2104.03245 [hep-ph]].
- [40] H. X. Wang, L. Wang and Y. Zhang, [arXiv:2104.03242 [hep-ph]].
- [41] M. Cadeddu, N. Cargioli, F. Dordei, C. Giunti and E. Picciau, [arXiv:2104.03280 [hep-ph]].

- [42] E. J. Chun and T. Mondal, [arXiv:2104.03701 [hep-ph]].
- [43] G. Arcadi, Á. S. De Jesus, T. B. De Melo, F. S. Queiroz and Y. S. Villamizar, [arXiv:2104.04456 [hep-ph]].
- [44] T. Li, M. A. Schmidt, C. Y. Yao and M. Yuan, [arXiv:2104.04494 [hep-ph]].
- [45] D. Borah, M. Dutta, S. Mahapatra and N. Sahu, [arXiv:2104.05656 [hep-ph]].
- [46] S. Zhou, [arXiv:2104.06858 [hep-ph]].
- [47] N. Aghanim *et al.* [Planck Collaboration], arXiv:1807.06209 [astro-ph.CO].
- [48] E. Aprile *et al.* [XENON Collaboration], Phys. Rev. Lett. **121**, no. 11, 111302 (2018) [arXiv:1805.12562 [astro-ph.CO]].
- [49] C. Amole *et al.* [PICO Collaboration], Phys. Rev. D **100**, no. 2, 022001 (2019) [arXiv:1902.04031 [astro-ph.CO]].
- [50] E. Aprile *et al.* [XENON Collaboration], Phys. Rev. Lett. **122**, no. 14, 141301 (2019) [arXiv:1902.03234 [astro-ph.CO]].
- [51] F. Bishara, J. Brod, B. Grinstein and J. Zupan, JCAP **02**, 009 (2017) [arXiv:1611.00368 [hep-ph]].
- [52] F. Bishara, J. Brod, B. Grinstein and J. Zupan, JHEP **11**, 059 (2017) [arXiv:1707.06998 [hep-ph]].
- [53] F. Bishara, J. Brod, B. Grinstein and J. Zupan, [arXiv:1708.02678 [hep-ph]].
- [54] J. Brod, A. Gootjes-Dreesbach, M. Tammaro and J. Zupan, JHEP **10**, 065 (2018) [arXiv:1710.10218 [hep-ph]].
- [55] J. Brod, B. Grinstein, E. Stamou and J. Zupan, JHEP **02**, 174 (2018) [arXiv:1801.04240 [hep-ph]].
- [56] F. Bishara, J. Brod, B. Grinstein and J. Zupan, JHEP **03**, 089 (2020) [arXiv:1809.03506 [hep-ph]].
- [57] A. L. Fitzpatrick, W. Haxton, E. Katz, N. Lubbers and Y. Xu, JCAP **02**, 004 (2013) [arXiv:1203.3542 [hep-ph]].
- [58] N. Anand, A. L. Fitzpatrick and W. C. Haxton, Phys. Rev. C **89**, no.6, 065501 (2014) [arXiv:1308.6288 [hep-ph]].
- [59] R. H. Helm, Phys. Rev. **104**, 1466-1475 (1956).
- [60] M. Lisanti, [arXiv:1603.03797 [hep-ph]].
- [61] P. A. Zyla *et al.* (Particle Data Group), Prog. Theor. Exp. Phys. **2020**, 083C01 (2020).

- [62] Q. H. Cao, E. Ma and G. Rajasekaran, Phys. Rev. D **76**, 095011 (2007) [arXiv:0708.2939 [hep-ph]].
- [63] D. Aristizabal Sierra, J. Kubo, D. Restrepo, D. Suematsu and O. Zapata, Phys. Rev. D **79**, 013011 (2009) [arXiv:0808.3340 [hep-ph]].
- [64] S. Bhattacharya, N. Sahoo and N. Sahu, Phys. Rev. D **93**, no. 11, 115040 (2016) [arXiv:1510.02760 [hep-ph]].
- [65] A. G. Hessler, A. Ibarra, E. Molinaro and S. Vogl, JHEP **1701**, 100 (2017) [arXiv:1611.09540 [hep-ph]].
- [66] M. A. Díaz, N. Rojas, S. Urrutia-Quiroga and J. W. F. Valle, JHEP **1708**, 017 (2017) [arXiv:1612.06569 [hep-ph]].
- [67] A. Ahriche, A. Jueid and S. Nasri, Phys. Rev. D **97**, no. 9, 095012 (2018) [arXiv:1710.03824 [hep-ph]].
- [68] B. Barman, S. Bhattacharya, P. Ghosh, S. Kadam and N. Sahu, Phys. Rev. D **100**, no. 1, 015027 (2019) [arXiv:1902.01217 [hep-ph]].
- [69] S. Bhattacharya, P. Ghosh, N. Sahoo and N. Sahu, Front. in Phys. **7**, 80 (2019) [arXiv:1812.06505 [hep-ph]].
- [70] Y. Cai, J. Herrero-García, M. A. Schmidt, A. Vicente and R. R. Volkas, Front. in Phys. **5**, 63 (2017) [arXiv:1706.08524 [hep-ph]].
- [71] P. F. de Salas, D. V. Forero, C. A. Ternes, M. Tortola and J. W. F. Valle, Phys. Lett. B **782**, 633 (2018) [arXiv:1708.01186 [hep-ph]].
- [72] G. Belanger, F. Boudjema, A. Pukhov and A. Semenov, Comput. Phys. Commun. **180**, 747 (2009) [arXiv:0803.2360 [hep-ph]].
- [73] G. Arcadi, A. Djouadi and M. Raidal, arXiv:1903.03616 [hep-ph].
- [74] A. Alves, A. Berlin, S. Profumo and F. S. Queiroz, Phys. Rev. D **92**, no. 8, 083004 (2015) [arXiv:1501.03490 [hep-ph]].
- [75] P. Ball and R. Zwicky, Phys. Rev. D **71**, 014029 (2005) [arXiv:hep-ph/0412079 [hep-ph]].
- [76] D. Rodríguez Pérez [Belle-II], Prospects for τ Lepton Physics at Belle II, [arXiv:1906.08950 [hep-ex]].
- [77] A. Belyaev, N. D. Christensen and A. Pukhov, Comput. Phys. Commun. **184**, 1729 (2013) [arXiv:1207.6082 [hep-ph]].
- [78] C. Arina and M. E. Cabrera, JHEP **04**, 100 (2014) [arXiv:1311.6549 [hep-ph]].

- [79] P. N. Bhattiprolu and S. P. Martin, *Phys. Rev. D* **100**, no.1, 015033 (2019) [arXiv:1905.00498 [hep-ph]].